Article:
Ng, C.T. and Susmel, L. (2020) Notch static strength of additively manufactured acrylonitrile butadiene styrene (ABS). Additive Manufacturing, 34. 101212. ISSN: 2214-8604

https://doi.org/10.1016/j.addma.2020.101212

Notch Static Strength of Additively Manufactured Acrylonitrile Butadiene Styrene (ABS)

Chin Tze Ng, Luca Susmel

Department of Civil and Structural Engineering, the University of Sheffield,
Mappin Street, Sheffield S1 3JD, UK

ABSTRACT

The present theoretical/experimental investigation deals with the problem of performing the static assessment of notched components made of additively manufactured Acrylonitrile Butadiene Styrene (ABS). The notch strength of this 3D-printed material was investigated by testing a large number of specimens, with the experiments being run not only under tension, but also under three-point bending. The samples contained geometrical features of different sharpness and were manufactured (flat on the build plate) by changing the printing direction. Being supported by the experimental evidence, the hypothesis was formed that the mechanical response of 3D-printed ABS can be modelled effectively by treating it as a material that is linear-elastic, brittle, homogenous and isotropic. This simplifying hypothesis allowed the Theory of Critical Distances to be employed also to assess static strength of 3D-printed ABS containing geometrical features. The validation exercise based on the experimental results being generated demonstrates that this theory is highly accurate, with its use leading to predictions falling mainly within an error interval of about ±20%. This level of accuracy is certainly satisfactory especially because this static assessment methodology can be used in situations of engineering relevance by making use of the results obtained by solving standard linear-elastic Finite Element models.

Keywords: additive manufacturing, Acrylonitrile Butadiene Styrene (ABS), Notch, Critical Distance.

Nomenclature

a, B, W	dimensions of the C(T) specimens according to ASTM D5045–14
E	Young's modulus
F_f	failure force
K_c	fracture toughness
K_{IC}	plane strain fracture toughness
L	critical distance
Oθr	polar coordinates
Oxy	local system of coordinates
P_{max}, P_Q	forces determined according to ASTM D5045-14
R	notch root radius
S_D	standard deviation
t	specimen's thickness
w_n, w_g	net and gross width
θ_p	manufacturing angle
$\sigma_{0.1\%}$	0.1% proof stress
σ_1	maximum principal stress
σ_{eff}	effective stress
σ_{UTS}	ultimate tensile strength
σ_x, σ_y, τ_{xy}	local stress components
σ_Y	yield stress
α	notch opening angle

1. Introduction

Acrylonitrile butadiene styrene (ABS) – $(C_8H_8C_4H_6C_3H_3N)_n$ - is a thermoplastic polymer that is widely used to manufacture lightweight, rigid components including automotive parts, pipes and protective headgear. As an engineering polymer, ABS is characterised by good mechanical properties, high impact strength and remarkable resistance to corrosion.

As far as situations of industrial interest are concerned, objects of ABS are still made mainly via injection moulding. However, together with polylactide (PLA) and thermoplastic polyurethane (TPU), ABS is a polymer that can be 3D-printed (at low cost) through those off-the-shelf 3D-printers that make use of the Fused Filament Fabrication (FFF) technique.

If attention is focussed on the mechanical properties of FFF-manufactured ABS, much experimental evidence [1-21] suggests that its overall mechanical behaviour is influenced by numerous technological variables that include, amongst others: layer thickness, infill level, printing rate, feed rate, temperature of the build plate, extrusion temperature, diameter of the filament, diameter of the nozzle, and printing direction. In this context, given the different parameters that influence the mechanical response of 3D-printed ABS, certainly the manufacturing orientation plays a role of primary importance [21]. For instance, as per Fig. 1a, the ultimate tensile strength, σ_{UTS}, and the yield stress, σ_Y, of ABS 3D-printed vertically on the build plate are seen to be lower than the corresponding mechanical properties obtained by manufacturing the specimens either on-edge or flat.

As long as objects of ABS are 3D-printed flat on the build plate, their overall mechanical behaviour is affected markedly by the value set for the raster angle (Fig. 1b). As to this aspect, the graphs of Fig. 1b make it evident that ultimate tensile stress, σ_{UTS}, flexural strength, σ_{fs}, yield stress, σ_Y, and Young's Modulus, E, of FFF-manufactured ABS decrease as the material meso-structure moves from lay-ups being mainly dominated by 3D-printed filaments at about 0° to lay-ups whose mechanical response is mainly governed by filaments at about 90°. This well-known behaviour is to be ascribed to the particular cracking processes that are observed in FFF-manufactured polymers. In particular, in these 3D-printed materials final breakage is seen to take place as a result of three distinct failure processes, i.e. (i) de-bonding between adjacent filaments, (ii) de-bonding between adjacent layers and (iii) rectilinear cracking of the filaments [1, 22, 23]. Accordingly, when the material meso-structure is dominated by 3D-printed filaments at about 90°, the overall strength of the material itself mainly depends on the bonding forces. Therefore, since, by their nature, these bonding forces result in a lower strength capacity than the one which associated with the axial mechanical strength of the extruded filaments, lay-ups with filaments mainly at 90° are characterised by a lower mechanical performance compared to the one obtained from meso-structures mainly based on 0°-oriented filaments. However, in spite of these complexities, the diagrams of Fig. 1b make it clear that both strength and stiffness of additively manufactured ABS are comparable with the corresponding mechanical properties that are obtained via classic, conventional injection moulding (IM). This experimental evidence further demonstrates that, as long as the key manufacturing variables are set correctly, FFF-based additive manufacturing can be used in situations of industrial interest to manufacture objects of ABS that are in any case characterised by good mechanical properties.

Turning back to 3D-printing technologies, one of the key features of additive manufacturing is that components with intricate shapes can be manufactured by reaching a remarkable level of

accuracy in terms of dimensions. However, from a static strength viewpoint, the presence of intricate geometrical features leads to localised stress concentration phenomena that have an inevitable detrimental effect on the strength of the components themselves. These considerations should make it clear that, to make the most of additive manufacturing, engineers need simple, reliable design tools capable of accurately performing the static assessment of 3D-printed materials containing geometrical features of all kinds (here termed "notches").

As per the literature review briefly discussed above, much experimental/theoretical work has already been done in order to understand and model the mechanical behaviour of plain (i.e., un-notched) 3D-printed ABS. In contrast, so far the problem of designing additively manufacture ABS containing notches has never been studied systematically before. Therefore, in this challenging scenario, this paper ambitiously aims at filling up this knowledge gap by investigating whether the Theory of Critical Distances [24] can successfully be used also to predict the static strength of notched 3D-printed ABS.

2. Experimental details

The specimens sketched in Fig. 2 were manufactured by using FFF-based 3D-printer Ultimaker 2 Extended+ and grey filaments of PRIMA 750g ABS having diameter equal 2.85mm. The used extrusion nozzle had diameter equal to 0.4 mm. During manufacturing the temperature of the nozzle was kept equal to 255˚C, whereas the temperature of the build plate to 90˚C. All the specimens were manufactured at a printing rate of 30 mm/s. The level of density was set equal to 100%, the height of the layers equal to 0.1 mm, and the thickness of the shell equal to 0.4 mm. With regard to the latter technological parameter, the thickness of the shell was set equal to the diameter of the nozzle being to minimise the formation of voids and defects at the interface between filling material and shell.

According to the sketch of Fig. 3a, both the plain and the notched samples were fabricated flat on the build-plate. In order to obtain different material lay-ups, the specimens were manufactured by making the manufacturing angle, θ_p, vary in the ranges 0˚-90˚ for the plain and 0˚-45˚ for the notched specimens. As shown in Fig. 3a, θ_p was the angle between the principal printing direction and the specimens' longitudinal axes, with the principal printing direction being perpendicular to the front command panel. Since the used 3D-printer extruded the filaments forming the filling volume always at ±45˚ to the principal manufacturing direction, setting angle θ_p equal either to 0˚ or to 90˚ returned specimens having a ±45˚ lay-up (Fig. 3a). Using a similar stratagem, specimens with a -15˚/+75˚ lay-up were then fabricated by taking θ_p equal to both 30˚ and 60˚, whereas samples with a 0˚/+90˚ lay-up were manufactured by taking θ_p equal to 45˚ (Fig. 3a).

According to Fig. 2, the un-notched specimens as well as the notched samples had thickness equal to 4mm. The actual dimensions of the specimens that are listed in Tables 1 to 6 were measured by using a high-precision calliper and an optical microscope.

The plain specimens (Fig. 2a) and the samples containing two opposite notches (Figs 2c to 2e and Figs 2i to 2l) were tested under axial loading. In contrast, the samples containing single notches were tested under three point bending, with the span between the two lower supports being set equal to 60 mm for the specimens with single open notches (Figs 2m to 2o) and to 50 mm for the other bending samples (Figs 2f to 2h).

According to the classical analytical framework due to Williams [25], the notch opening angle, α, is a geometrical parameter that influences the distribution of the linear-elastic stress fields in the vicinity of the notch itself. In particular, Williams's solution suggests that, in linear-elastic, homogenous and isotropic materials, the effect of the opening angle can be disregarded with a little loss of accuracy as long as α is lower than about 100°. In contrast, when the opening angle becomes larger than about 100°, α is seen to affect not only the profile, but also the magnitude of the corresponding local linear-elastic stress distributions [26]. Accordingly, to accurately investigate the static behaviour of 3D-printed ABS in the presence of stress concentration phenomena, a number of tensile specimens (Figs 2i to 2l) as well as of bending samples (Figs 2m to 2o) were then fabricated by taking opening angle α equal to 135° (here termed "open notches").

The C(T) specimens were FFF-fabricated as recommended by ASTM D5045–14 [27], with the thickness varying in the range 7-30 mm - the technical drawing reported in Fig. 2b shows solely a C(T) specimen having thickness equal to 30 mm.

By using a Shimadzu axial machine, all the specimens being sketched in Fig. 2 were tested up to complete breakage, with the displacement rate being set invariably equal to 2 mm/min. Local axial strains in the smooth specimens were measured and gathered during testing at a frequency of 10 Hz through an extensometer having gauge length equal to 50 mm. Fig. 3b shows a few examples of the different experimental set-ups that were employed to test the specimens sketched in Fig. 2.

The results being generated following the experimental procedures summarised in the present section are listed in Tables 1 to 6. The meaning of the symbols used in these tables is explained in the Nomenclature.

3. Ultimate tensile strength, 0.1% proof stress, and Young's modulus

The stress vs. strain diagrams seen in Fig. 4 show the typical mechanical response displayed by the plain specimens (Fig. 2a) when tested under tension.

As to the observed mechanical response, initially, it is interesting to point out that, according to the diagrams of Fig. 4, the stress-strain behaviour was seen to be almost linear up to the maximum stress that was recorded during testing, with this holding true irrespective the value of manufacturing angle θ_p. Therefore, according to the behaviour being observed experimentally, the hypothesis can be formed that the mechanical response of the 3D-printed ABS being tested can be modelled effectively by simply linearizing the stress-strain law up to final breakage.

Focussing attention on the ductility level that characterises the different material lay-ups, Figs 4a and 4e show that the stress-strain curves associated with the samples FFF-fabricated by taking θ_p equal to 0° and 90° are those displaying the largest level of non-linear deformations. In contrast, in the samples with either a -15°/+75° lay-up (Figs 4b and 4d) or a 0°/+90° lay-up (Fig. 4c) final breakage occurred as soon as the stress reached its maximum value. In this context, it is important to point out also that, independently of the value being set for manufacturing angle θ_p, failures were never preceded by any evident localised necking.

The charts of Fig. 5 summarise the mechanical response of the FFF-printed polymer being tested in terms of elastic modulus, E, 0.1% proof stress, $\sigma_{0.1\%}$, and ultimate tensile strength, σ_{UTS}. For the sake of clarity and completeness, the same values are also listed in Tab. 1 for any individual test that was run. The graphs of Fig. 5 make it clear that the mechanical response of the 3D-printed ABS under investigation was clearly affected by the manufacturing direction, although, as expected [22, 23], the influence of angle θ_p was seen to be little. Further, the diagrams of Fig. 5 also demonstrate that the stress-strain behaviour of those specimens manufactured by setting θ_p equal to 0° and 30° was comparable to the mechanical response associated with the samples manufactured with θ_p equal to 60° and 90°, respectively. Accordingly, in order to reduce the number of specimens used to investigate the static strength of the tested 3D-printed ABS in the presence of stress concentration phenomena, the notched specimens sketched in Fig. 2 were manufactured by setting angle θ_p solely equal to 0°, 30°, and 45°.

Turning back to the strain-strain behaviour of the un-notched material, if the effect of manufacturing angle θ_p is neglected, then the average values for the three relevant mechanical properties are as follows: E=1590 MPa, $\sigma_{0.1\%}$=20.8 MPa, and σ_{UTS}=23.0 MPa. According to the diagrams reported in Fig. 5, the mechanical properties measured by testing specimens manufactured by taking angle θ_p in the range 0°-90° all fall within two standard deviation of the mean (i.e., $\pm 2S_D$ in the charts of Fig. 5). While, strictly speaking, angle θ_p does affect the overall mechanical response of the tested 3D-printed ABS, these results further confirm that for design

purposes the influence of the material lay-up on E, $\sigma_{0.1\%}$ and σ_{UTS} can be disregarded, with this simplifying assumption resulting just in a marginal loss of accuracy.

Subsequently, in order to investigate the effect of the material lay-up on the cracking behaviour of the 3D-printed ABS being tested, attention was focused not only on the crack propagation phase, but also on the crack initiation process. The pictures seen in Fig. 6a show some examples of the crack paths that were observed in the plain samples being tested. In particular, irrespective of the value of angle θ_p, the cracks were seen to initiate always on material planes being almost normal to the loading direction. This Mode I stress-dominated initiation process led to initial cracks having length approaching the thickness of the shell (i.e., having length approaching 0.4 mm). The subsequent growth phase was seen to occur on zig-zag paths following the directions of the extruded filling filaments.

According to the observed cracking behaviour, it is possible to conclude by pointing out that the propagation of the cracks in the tested 3D-printed ABS was the result of three failure mechanisms, i.e., de-bonding between adjacent filaments, de-bonding between adjacent layers and, finally, rectilinear cracking of the extruded filaments.

4. Fracture toughness

The plane strain fracture toughness, K_{IC}, of the 3D-printed ABS being studied was measured experimentally via C(T) specimens (Fig. 2b) designed and tested by following the pertinent ASTM recommendations [27]. The force vs. displacement curves generated by testing the C(T) samples are shown in Fig. 4f. The profile of these curves makes it evident that the mechanical response of the C(T) specimens made of FFF-fabricated ABS was similar to the one usually displayed by C(T) specimens of conventional polymeric materials [27]. It is also interesting to observe that some of the curves show an evident initial "jump". This has to be ascribed to the physiological mechanical adjustment of the testing apparatus occurring at the beginning of those tests showing this initial discontinuity in the force vs. displacement curve. However, this problem was compensated by post-processing the obtained curves according to the ASTM procedure [27].

As discussed in the previous Section, in the un-notched samples with $\theta_p \neq 45^\circ$ the cracks were seen to grow along zig-zag paths whose profiles followed the orientation of the extruded filaments. This means that, at a mesoscopic level, in those specimens with $\theta_p \neq 45^\circ$ the crack propagation process was always driven by local mechanisms that were Mixed-Mode I/II dominated. In contrast, since the deposited filaments in these specimens were either normal or parallel to the loading direction, solely in the specimens with $\theta_p = 45^\circ$ the cracking behaviour was governed by a pure Mode I failure

mechanism. This explains why all the C(T) specimens being tested were FFF-fabricated by setting manufacturing angle θ_p invariably equal to 45°.

Another important aspect is that, contrary to what is suggested by ASTM D5045-14 [27], the C(T) specimens were tested without introducing any pre-crack. This was done deliberately so that the fracture toughness for the 3D-printed ABS under investigation could be determined by accounting also for the effect of the 0.4 mm shell.

Fig. 6b show an example of the crack initiation (right) and crack propagation (left) processes as they were observed in the C(T) samples. This figure makes it evident that, as planned, the cracks grew along the notch bisector, with the propagation process being purely Mode I-driven. In this context, it can be pointed out also that in the C(T) specimens the cracks tended to initiate slightly away from the notch tip, with the initial propagation occurring, in the vicinity of the notch tip itself, at the interface between the shell and the filling material. This can be ascribed to the way the material was deposited near the notch, with this stress concentrator being very sharp.

The results generated by testing the C(T) specimens are listed in Tab. 6 in terms of maximum force recorded during testing, P_{max}, reference force, P_Q, extrapolated according the procedure recommended by ASTM D5045-14 [27], and, finally, fracture toughness, K_C. This table makes it evident, in contrast with the trend that is usually displayed by conventional plastic materials, K_C for the 3D-printed ABS being tested was seen not to decrease as the thickness increased from about 7 mm up to about 30 mm. This clearly suggests that more theoretical/experimental work needs to be done to understand and model the effect of geometry and thickness on the fracture toughness of additively manufactured ABS.

Having highlighted these important aspects and limitations, ultimately the plain fracture toughness for the 3D-printed polymer under investigation was then estimated by averaging the results from the three tests run by using the C(T) specimens with nominal thickness, B, equal to 30 mm. This straightforward calculation returned an average value for K_{IC} equal to 2.6 MPa·m$^{1/2}$.

To conclude, it is important to point out that, according to the empirical rule suggested by ASTM D5045-14 [27], the fracture toughness values obtained from specimens with thickness equal to about 30 mm were determined under almost-fully-developed plane strain conditions.

5. Mechanical behaviour in the presence of notches

The diagrams seen in Fig. 7 show some force vs. displacement curves as well as some bending moment vs. deflection curves that were obtained from the notched specimens of Fig. 2 tested under tension as well as under bending. As an example, the curves plotted in the diagrams of Fig.

7 refer to the first test that was run for any notch profile/loading configuration being considered in the present investigation.

The mechanical behaviour displayed by the diagrams of Fig. 7 suggests that, in the notched specimens, breakage always took place as soon as the applied force or moment reached its maximum value, with this holding true irrespective of profile and sharpness of the notch.

Focusing attention on the results generated under axial loading, the force vs. displacement curves shown in Figs 7a to 7f were all formed of two linear branches, where, compared to the first linear part, the second branch was always less steep. Further, the change in the slope always occurred around 0.25 mm, with this holding true irrespective of notch sharpness and value of the notch opening angle. Clearly, it is very difficult to find a physical explanation for this interesting phenomenon. However, this change in the slope could be ascribed to the fact that, in the presence of notches, the initial deformation was mainly due to a relative displacement between adjacent filaments. This initial sliding-based straining mechanism was then followed by a deformation process mainly depending on the tensile properties of the individual filaments forming the bulk material. The different stiffness associated with these two deformation mechanisms would explain the reason why the force displacement curves seen in Figs 7a to 7F show two distinct values of the slop. However, this is just a possible explanation and, certainly, more work needs to be done to clarify this interesting aspect.

As far as the results under three-point bending are concerned, the diagrams reported in Figs 7g to 7l show that, as expected, all the bending moment vs. deflection curves displayed an initial non-linear behaviour due to the rig's mechanical adjustment occurring at the beginning of any test. This initial non-linear response was then followed by a predominantly linear behaviour up to final fracture.

All the results generated by testing the notch specimens sketched in Fig. 2 are listed in Tables 2 to 5 in terms of maximum force, F_f, recorded during testing. It is useful to recall here that, as briefly mentioned in Section 3, the notched samples were FFF-fabricated by setting θ_p solely equal to 0°, 30°, and 45°. This was done because, as per the results obtained by testing the plain specimens (see Fig. 5), the mechanical behaviours for θ_p=0° and for θ_p=30° were seen to be very similar to those obtained by taking θ_p equal to 90° and 60°, respectively. This allowed us to reduce markedly the number of specimens that had to be manufactured and tested to study the notch static behaviour of the 3D-printed polymer under investigation.

The failure forces, F_f, reported in Tables 2 to 5 suggest that the static strength of the notched specimens tested both under tension and under bending was slightly affected by printing angle

θ_p. In particular, the magnitude of the failure force was seen to decrease as angle θ_p increased, with this effect being more evident in the notched samples loaded in bending.

Another important aspect that is worth pointing out here is that the sharpest notches were not always characterised by the lowest strength. In particular, Table 7 reports the average value and the standard deviation, S_D, of the failure force determined from the three tests that were run to investigate any considered notch/loading configurations. Table 7 confirms that the 3D-printed polymer under investigation was characterised by a very low notch sensitivity. This implies that, in theory, the standard nominal stress based approach would allow notched components of 3D-printed ABS to be designed by always reaching an acceptable level of structural safety. However, one of the key features of additive manufacturing is that, by its nature, this technology is suitable for fabricating objects with very complex geometries. As far as components with complex three-dimensional shapes are concerned, it is well-known that it is never straightforward to define nominal sections unambiguously, with this making difficult for the nominal stress based approach to be used successfully under these specific circumstances. In this setting, the obvious alternative is then solving Finite Element (FE) models so that the local peak stresses can be determined at the hot-spots. Unfortunately, directly using hot-spot stresses with materials characterised by a low notch sensitivity would systematically result in over-designed components, i.e., in components that are bigger and heavier than necessary. Thus, a reliable design tool is needed to perform accurately the static assessment of 3D-printed objects with complex shape. This key aspect will be addressed in the next sections as attempting to extend the use of the Theory of Critical Distances to the static assessment of notched components of FFF-manufactured ABS.

Turning back to Table 7, another important aspect is that, according to the reported values of the average failure forces, notches with very large root radii may even have a beneficial effect, with the associated strength being higher than the one displayed by the un-notched material. Having said that, certainly, it would be worth investigating this interesting aspect in detail. However, since this specific problem was out of the scopes of the research work summarised in the present work, our attention was focussed solely on the effect of stress concentrators having relatively small root radii.

The matrices of failures reported in Figs 8 and 9 show the crack initiation process in the notched samples subjected to tension and to three-point bending, respectively. In accordance with the cracking behaviour that was observed in the plain samples (Fig. 6a), in the presence of stress concentrators as well cracks were seen to initiate, at the notch tips, on material planes that were almost perpendicular to the loading direction. These embryonic cracks having length approaching 0.4 mm (i.e., equal to about the shell thickness) led to a subsequent propagation process occurring

on zig-zag paths whose profile depended on the material lay-up. To conclude, it can be said that also in the presence of stress concentrators the cracking behaviour of 3D-printed ABS was seen to be due to the combined effect of de-bonding (between adjacent filaments as well as between adjacent layers) and rectilinear cracking.

6. Fundamental of the Theory of Critical Distances

The mechanical behaviour displayed by the additively manufactured ABS under investigation (Figs 4 and 5) allows the following two simplifying engineering hypotheses to be formed:

- additively manufactured ABS can be modelled as an homogenous and isotropic material;
- additively manufactured ABS behaves like a linear-elastic, brittle material.

Clearly, these two simplifying assumptions are valid as long as components/objects are 3D-printed flat on the build plate (Figs 1a and 3a). Having set this design scenario, the static strength of notched components made of 3D printed ABS can then attempted to be assessed by taking full-advantage of the Theory of Critical Distances (TCD) [24]. The key features of this powerful design tool will be reviewed briefly in what follows.

According to the TCD, static strength is estimated via an effective stress, σ_{eff}, whose magnitude depends on the local linear-elastic stress field acting on the material in the notch tip region. In this setting, a notched component is assumed not to break as long as the following condition is assured [28-30]:

$$\sigma_{eff} \leq \sigma_{UTS} \tag{1}$$

where σ_{UTS} is the conventional ultimate tensile strength that can be determined experimentally by running standard tensile tests [28]. The TCD effective stress instead is calculated by defining a critical distance whose length depends on the primary source of microstructural heterogeneity. In particular, the TCD material length is seen to be about an order of magnitude larger than the size of the dominant microstructural features [31].

Independently of the strategy being adopted to calculate σ_{eff}, the TCD assumes that the critical distance can directly be derived from the following well-known relationship [28, 32, 33]:

$$L = \frac{1}{\pi}\left(\frac{K_{IC}}{\sigma_{UTS}}\right)^2, \tag{2}$$

where K_{IC} is the plane strain fracture toughness. Since, according to definition (2), L is derived from two material properties (i.e. σ_{UTS} and K_{IC}), the TCD critical distance is in turn a material property so this length does not depend on profile and sharpness of the stress raiser being designed [24].

As soon as the material characteristic length is known, the TCD effective stress can be determined according to either the Point, the Line, or the Area Method [24].

The Point Method (PM) is the simplest formalisation of the TCD. It postulates that σ_{eff} is equal to the linear-elastic stress at a distance from the notch tip equal to L/2. As per Figs 10a and 10b, the PM effective stress can then be defined mathematically as follows:

$$\sigma_{eff} = \sigma_y \left(\theta = 0^{\circ}, \mathrm{r} = \frac{L}{2}\right) \tag{3}$$

A second way to apply the TCD is by averaging the linear-elastic stress along the notch bisector over a distance equal to 2L [24, 28]. This formalisation of the TCD is known as the Line Method (LM) and it can be expressed mathematically as follows (Fig. 10c):

$$\sigma_{eff} = \frac{1}{2L}\int_0^{2L} \sigma_y(\theta = 0^{\circ}, \mathrm{r}) \cdot dr \tag{4}$$

The third formalisation of the TCD considered in what follows is usually referred to as the Area Method (AM). As per this approach's *modus operandi*, the effective stress is determined by averaging the linear-elastic stress over a semi-circle that is centred at the notch tip and has radius equal to L, i.e. (Fig. 10d) [24, 34]:

$$\sigma_{eff} = \frac{4}{\pi L^2}\int_0^{\frac{\pi}{2}}\int_0^{L} \sigma_1(\theta, \mathrm{r}) \cdot r \cdot dr \cdot d\theta \tag{5}$$

Finally, the most complex and laborious formalisation of the TCD postulates that the effective stress can also be calculated by averaging the linear-elastic maximum principal stress over a hemisphere with radius equal to 1.54L and centred at the notch tip [35].

As to the accuracy of the TCD, it can be recalled here that this linear-elastic design approach is seen to be successful in assessing static strength also of ductile metals containing a variety of geometrical features and subjected to uniaxial/multiaxial loading [36-39]. This aspect is very

important because this confirms that, by its nature, the linear-elastic TCD is capable of directly accommodating any material non-linearities into a linear-elastic constitutive law [40].

In this context, it is important to remember also that the actual value of the TCD reference strength depends on the mechanical/cracking behaviour displayed by the material under investigation. In particular, for those materials whose mechanical response is characterised by a certain degree of non-linearity, the reference failure stress can take a value that is larger than σ_{UTS} [24, 36]. This specific phenomenon is observed not only in standard ductile materials such as metals [24, 37, 38], but also in quasi-brittle polymers such as polymethylmethacrylate [29, 30]. In contrast, the TCD reference strength is seen to be equal to σ_{UTS} for those materials having a linear stress-strain behaviour (for instance, in ceramics [28]) or, in any case, having a mechanical response that is characterised by a limited level of non-linearity (for instance, in fibre reinforced composites [32]). Further, the TCD reference strength is seen to be different from σ_{UTS} also in those circumstances in which local stress concentration phenomena lead to failure mechanisms that are different from those characterising the cracking behaviour of the plain material [26].

These considerations suggest that, given the slightly non-linear mechanical behaviour displayed by the FFF-manufactured polymer under investigation (Fig. 4), the TCD may be attempted to be applied also by adopting a reference strength higher than σ_{UTS}. However, this was not done simply because much experimental evidence [29, 30, 32] confirms that, for those material whose mechanical response is characterised by a limited level of non-linearity, accurate estimates can be obtained by simply taking the TCD reference strength equal to σ_{UTS}. Accordingly, in the next section the static strength of the notched specimens being tested will be assessed by applying the TCD as briefly reviewed in the present section.

7. Accuracy of the TCD in estimating notch static strength of 3D-printed ABS

To use the TCD effective stress to assess the static strength of the notched samples shown in Fig. 2, the local linear-elastic stress fields in the notch regions were estimated by using commercial code ANSYS®. This was done by solving simple bi-dimensional linear-elastic Finite Element (FE) modes, with the mesh density in the highly stressed regions being increased progressively until convergence occurred. Finally, the numerical solutions were calculated by setting Young's modulus equal to 1590 MPa (Fig. 5a) and Poisson's ratio to 0.36 [6].

A TCD critical distance, L, equal to 4.1 mm was estimated according to definition (2) by taking σ_{UTS}=23 MPa and K_{IC}=2.6 MPa·m$^{1/2}$. This value for L allowed us to post-process the notch results being generated according to the PM and the AM. The LM instead could not be used because the integration length (i.e., 2L=8.2 mm) was larger than half net-width [24].

The TCD effective stress, σ_{eff}, vs. manufacturing angle, θ_p, diagrams reported in Figs 10e and 10f summarise the level of accuracy that was reached by using the TCD in terms of the PM and AM, respectively. In the above charts the error was calculated as:

$$Error = \frac{\sigma_{eff} - \sigma_{UTS}}{\sigma_{UTS}} \ [\%]$$

According to this definition, a positive value for the error denotes conservative estimates, whereas, obviously, non-conservative predictions return negative errors.

The diagrams reported Figs 10e and 10f confirm that, as for other conventional engineering materials [24, 28-33, 36-40], the systematic usage of the PM and LM returned estimates mainly falling with in an error interval of ±20%. This result is certainly satisfactory, especially in light of the complex cracking behaviour that was displayed by the tested notched samples (see Figs. 6, 8 and 9).

8. Conclusions

Initially, a large number of tests were run to investigate the effect of notches having different profile and sharpness on the mechanical/cracking behaviour of FFF-manufactured ABS. The notched samples being tested were all manufactured flat on the build plate by making the manufacturing angle, θ_p, vary in the range 0°-45°. These specimens, containing not only conventional notches, but also open notches, were tested under tension as well as under three-point bending. Subsequently, all the notch results being generated were post-processed according to the TCD.

This systematic experimental/theoretical work allowed us to come to the following conclusions that strictly apply solely to objects of ABS additively manufactured flat on the build plate:

- in the absence of stress concentration phenomena, the mechanical response can be assumed to be linear up to final breakage, with this holding true irrespective of manufacturing angle value;
- as θ_p varies in the range 0°-90°, the relevant mechanical properties of 3D-printed ABS (i.e., elastic Modulus, E, 0.1% proof stress, $\sigma_{0.1\%}$, and ultimate tensile strength, σ_{UTS}) are seen to be all within two standard deviations of the mean;
- as far as 3D-printed ABS is concerned, an increase of the notch sharpness does not always result in a decrease of the static strength;
- the profile of the crack paths fully depends on the material lay-up;

- the fracture toughness appears to be influenced marginally by the thickness;
- the TCD has proven to be highly accurate also in assessing notch static strength of 3D-printed ABS, with its systematic usage resulting in predictions being within an error interval of about ±20%;
- more work needs to be done in order to investigate the notch effect in ABS additively manufactured vertically on the build plate;
- since 3D-printed ABS may be used also in applications that require resistance to impact and other high-rate loading, more work should be done also to investigate the strain-rate effects both in the absence and in the presence of notches.

Acknowledgments

Support for this work from the Faculty of Engineering of the University of Sheffield, Sheffield, UK, through the award of a SURE scheme scholarship is gratefully acknowledged.

References

[1] O. Es-Said, J. Foyos, R. Noorani, M. Mendelson, R. Marloth, B. Pregger, Effect of Layer Orientation on Mechanical Properties of Rapid Prototyped Samples. Mater. Manuf. Process. 15(1) (2000) 107-122.

[2] S. Ahn, M. Montero, D. Odell, S. Roundy, P. Wright, Anisotropic material properties of fused deposition modeling ABS. Rapid Prototyp. J. 8(4) (2002) 248-257.

[3] C. Ziemian, M. Sharma, S. Ziemian, Anisotropic Mechanical Properties of ABS Parts Fabricated by Fused Deposition Modelling, in: Mechanical Engineering, M. Gokcek (Ed.), InTech, 2012, pp. 159-180.

[4] S. Ziemian, M. Okwara, C. Ziemian, Tensile and fatigue behavior of layered acrylonitrile butadiene styrene. Rapid Prototyp. J. 21(3) (2015) 270-278.

[5] D. Cole, J. Riddick, J. Iftekhar, K. Strawhecker, N. Zander, 2016. Interfacial mechanical behavior of 3D printed ABS. J. Appl. Polym. Sci. 133(30), 43671. https://doi.org/10.1002/app.43671.

[6] J. Cantrell et al., Experimental characterization of the mechanical properties of 3D-printed ABS and polycarbonate parts. Rapid Prototyp. J. 23(4) (2017) 811-824.

[7] C. Koch, L. Van Hulle, N. Rudolph, Investigation of mechanical anisotropy of the fused filament fabrication process via customized tool path generation. Addit. Manuf. 16 (2017) 138-145.

[8] L. Li, Q. Sun, C. Bellehumeur, P. Gu, Composite Modelling and Analysis for Fabrication of FFF Prototypes with Locally Controlled Properties. J. Manuf. Process. 4(2) (2002) 129-141.

[9] B. Tymrak, M. Kreiger, J. Pearce, Mechanical properties of components fabricated with open-source 3-D printers under realistic environmental conditions. Mater. Design 58 (2014) 242-246.

[10] S. Raut, V. Jatti, N. Khedkar, T. Singh, Investigation of the Effect of Built Orientation on Mechanical Properties and Total Cost of FFF Parts. Procedia Materials Science 6 (2014) 1625-1630.

[11] M. Faes, E. Ferraris, D. Moens, Influence of Inter-layer Cooling time on the Quasi-static Properties of ABS Components Produced via Fused Deposition Modelling. Procedia CIRP 42 (2016) 748-753.

[12] A. Peterson, Review of acrylonitrile butadiene styrene in fused filament fabrication: A plastics engineering-focused perspective. Addit. Manuf. 27 (2019) 363-371.

[13] C. Casavola, A. Cazzato, V. Moramarco, C. Pappalettere, Orthotropic mechanical properties of fused deposition modelling parts described by classical laminate theory. Mater Des 90 (2016) 453–458.

[14] W. Wu, P. Geng, G. Li, D. Zhao, H. Zhang, J. Zhao, Influence of layer thickness and raster angle on the mechanical properties of 3D-Printed PEEK and a comparative mechanical study between PEEK and ABS. Materials 8 (2015) 5834–5846.

[15] I. Durgun, R. Ertan, Experimental investigation of FFF process for improvement of mechanical properties and production cost. Rapid Prototyp. J. 20 (2014) 228–235.

[16] B. Rankouhi, S. Javadpour, F. Delfanian, T. Letcher, Failure analysis and mechanical characterization of 3D printed ABS with respect to layer thickness and orientation. J. Fail. Anal. Prev. 16 (2016) 467–481.

[17] J.F. Rodríguez, J.P. Thomas, J.E. Renaud, Mechanical behavior of acrylonitrile butadiene styrene (ABS) fused deposition materials. Experimental investigation. Rapid Prototyp. J. 7 (2001) 148–58.

[18] B.H. Lee, J. Abdullah, Z.A. Khan, Optimization of rapid prototyping parameters for production of flexible ABS object. J. Mater. Process. Technol. 169 (2005) 54–61.

[19] J. F. Rodrıguez, J. P. Thomas, J. E. Renaud, Design of fused-deposition ABS components for stiffness and strength. J. Mech. Des. 125 (2003) 545–551.

[20] E. Kim, Y.J. Shin, S.H. Ahn, The effects of moisture and temperature on the mechanical properties of additive manufacturing components: fused deposition modelling. Rapid Prototyp J 22 (2016) 887–894.

[21] H. Ramezani Dana, F.Barbe, L.Delbreilh, M. Ben Azzouna, A. Guillet, T.Breteau, Polymer additive manufacturing of ABS structure: Influence of printing direction on mechanical properties. J. Manuf. Process. 44 (2019) 288-298.

[22] A.A. Ahmed, L. Susmel, A material length scale based methodology to assess static strength of notched additively manufactured polylactide (PLA). Fatigue Fract. Eng. Mater. Struct. 41 (2018) 2071-2098.

[23] A.A. Ahmed, L. Susmel, Static assessment of plain/notched polylactide (PLA) 3D-printed with different in-fill levels: equivalent homogenised material concept and Theory of Critical Distances. Fatigue Fract. Eng. Mater. Struct. 42 (2019) 883–904.

[24] D. Taylor, The Theory of Critical Distances: A New Perspective in Fracture Mechanics, Elsevier Ltd, Oxford, UK, 2007.

[25] M.L. Williams, Stress singularities resulting from various boundary conditions in angular cornersof plates in tension. J. Appl. Mech. 19 (1952) 526–528.

[26] P. Lazzarin, R. Tovo, A notch intensity factor approach to the stress analysis of welds. Fatigue Fract. Eng. Mater. Struct. 21 (1998) 1089–1103.

[27] ASTM D5045-14, Standard Test Methods for Plane-Strain Fracture Toughness and Strain Energy Release Rate of Plastic Materials, ASTM International, West Conshohocken, PA, 2014, www.astm.org.

[28] D. Taylor, Predicting the fracture strength of ceramic materials using the theory of critical distances. Eng. Fract. Mech. 71 (2004) 2407-2416.

[29] D. Taylor, M. Merlo, R. Pegley, M.P. Cavatorta, The effect of stress concentrations on the fracture strength of polymethylmethacrylate. Mater. Sci. Eng. A382 (2004) 288–294.

[30] L. Susmel, D. Taylor, The theory of critical distances to predict static strength of notched brittle components subjected to mixed-mode loading. Eng. Fract. Mech. 75 (2008) 534–550.

[31] D. Taylor, The Theory of Critical Distances: A link to micromechanisms. Theor. Appl. Fract. Mec. 90 (2017) 228–233

[32] J.M. Whitney, R.J. Nuismer, Stress Fracture Criteria for Laminated Composites Containing Stress Concentrations. J. Compos. Mater. 8 (1974) 253-65.

[33] R. Louks, H. Askes, L. Susmel, A simplified reformulation of the Theory of Critical Distances for rapid finite element design of notched materials against static loading. Mater. Des. 108 (2016) 769-779.

[34] S.D. Sheppard, Field effects in fatigue crack initiation: long life fatigue strength. Trans. ASME, J. Mech. Des. 113 (1991) 188-194.

[35] D. Bellett, D. Taylor, S. Marco, E. Mazzeo, J. Guillois, T. Pircher, The fatigue behaviour of three-dimensional stress concentrations. Int. J. Fatigue 27 (2005) 207-221.

[36] L. Susmel, D. Taylor, On the use of the theory of critical distances to predict static failures in ductile metallic materials containing different geometrical features, Eng. Fract. Mech. 75 (2008) 4410–4421.

[37] L. Susmel, D. Taylor, The theory of critical distances to estimate the static strength of notched samples of Al6082 loaded in combined tension and torsion. Part I: material cracking behaviour, Eng. Fract. Mech. 77 (2010) 452–469.

[38] L. Susmel, D. Taylor, The theory of critical distances to estimate the static strength of notched samples of Al6082 loaded in combined tension and torsion. Part II: multiaxial static assessment, Eng. Fract. Mech. 77 (2010) 470–478.

[39] A.A.H. Ameri, J.B. Davison, L. Susmel, On the use of linear-elastic local stresses to design steel arc welded joints against static loading, Eng. Fract. Mech. 136 (2015) 38-57.

[40] Li, W., Susmel, L., Askes, H., Liao, F., Zhou, T. Ductile fracture of Q460 steel: application of the Theory of Critical Distances. Eng. Fail. Anal. 70 (2016) 73–89.

List of Captions

Tables

Code	θ_P	w	t	F_f	E	$\sigma_{0.1\%}$	σ_{UTS}
	[°]	*[mm]*	*[mm]*	*[N]*	*[MPa]*	*[MPa]*	*[MPa]*
P0_1	0	14.93	4.00	1278	1519	19.2	21.4
P0_2	0	14.85	3.99	1286	1471	19.2	21.7
P0_3	0	14.86	3.95	1171	1410	17.9	19.9
P30_1	30	14.90	3.97	1427	1771	20.9	24.2
P30_2	30	14.82	3.96	1286	1727	21.0	21.9
P30_3	30	14.92	3.98	1550	1710	22.8	26.1
P45_1	45	14.83	3.93	1183	1669	19.4	20.3
P45_2	45	14.92	3.95	1198	1649	19.8	20.3
P45_3	45	14.91	4.01	1262	1483	19.1	21.1
P60_1	60	14.97	3.99	1359	1606	20.5	22.8
P60_2	60	14.92	3.95	1234	1662	19.3	20.9
P60_3	60	14.92	3.99	1244	1573	19.5	20.9
P90_1	90	14.92	3.94	1609	1486	24.0	27.4
P90_2	90	14.95	3.94	1648	1549	24.8	28.0
P90_3	90	14.95	3.97	1623	1556	24.1	27.3

Table 1. Summary of the experimental results generated by testing the plain specimens (Fig. 2a) under tensile loading.

Code	θ_P	R	w_n	w_g	t	F_f
	[°]	*[mm]*	*[mm]*	*[mm]*	*[mm]*	*[N]*
UB_0_1	0	2.93	15.11	24.71	3.93	1670
UB_0_2	0	2.94	15.12	24.74	3.96	1679
UB_0_3	0	2.96	15.16	24.82	3.95	1214
UB_30_1	30	2.95	15.11	24.80	3.95	1309
UB_30_2	30	2.90	15.09	24.83	3.91	1474
UB_30_3	30	2.94	15.05	24.86	3.92	1352
UB_45_1	45	2.97	15.13	24.91	3.94	1397
UB_45_2	45	2.94	15.18	24.81	3.93	1495
UB_45_3	45	2.91	15.12	24.88	3.96	1211
UI_0_1	0	0.97	15.28	24.77	3.95	1758
UI_0_2	0	0.94	15.21	24.65	3.96	1839
UI_0_3	0	0.92	15.26	24.71	3.94	1781
UI_30_1	30	0.92	15.23	24.74	3.90	1474
UI_30_2	30	0.92	15.28	24.71	3.91	1290
UI_30_3	30	0.93	15.13	24.78	3.88	1440
UI_45_1	45	0.99	15.22	24.70	3.98	1468
UI_45_2	45	0.96	15.19	24.70	4.02	1101
UI_45_3	45	0.98	15.25	24.72	3.96	1410
US_0_1	0	0.50	15.26	24.95	3.91	902
US_0_2	0	0.49	15.15	24.85	3.92	1106
US_0_3	0	0.49	15.23	24.87	3.98	1588
US_30_1	30	0.49	15.25	24.93	3.94	1191
US_30_2	30	0.50	15.26	24.90	3.96	1297
US_30_3	30	0.49	15.21	24.98	3.97	1176
US_45_1	45	0.53	15.16	24.90	3.94	1122
US_45_2	45	0.51	15.09	24.97	3.96	1182
US_45_3	45	0.50	15.07	24.91	4.00	1353

Table 2. Summary of the experimental results generated by testing the notched specimens (Figs 2c to 2e) under tensile loading.

Code	θ_P [°]	R [mm]	w_n [mm]	w_g [mm]	t [mm]	F_f [N]
OB_0_1	0	2.99	14.93	24.81	3.91	1262
OB_0_2	0	2.97	15.07	24.92	3.93	963
OB_0_3	0	3.01	14.99	24.93	3.99	1404
OB_30_1	30	3.02	15.03	24.80	4.00	1193
OB_30_2	30	2.97	15.01	24.83	3.99	1359
OB_30_3	30	2.98	15.10	25.01	4.01	1302
OB_45_1	45	3.00	14.99	24.96	4.03	1491
OB_45_2	45	2.98	15.00	24.89	4.01	1301
OB_45_3	45	2.98	14.96	24.87	3.92	1444
OI_0_1	0	1.02	14.99	24.86	4.03	1529
OI_0_2	0	1.01	14.94	24.78	4.00	1415
OI_0_3	0	1.03	14.99	24.89	3.99	1532
OI_30_1	30	1.00	14.95	24.91	3.97	1397
OI_30_2	30	1.01	14.93	24.81	3.95	1455
OI_30_3	30	0.98	14.98	24.92	4.02	1379
OI_45_1	45	0.98	14.99	24.78	3.99	1237
OI_45_2	45	1.02	14.91	24.76	4.03	1361
OI_45_3	45	1.01	15.00	24.87	4.01	1161
OS_0_1	0	0.48	15.09	24.74	4.00	1366
OS_0_2	0	0.47	15.12	24.81	3.96	1373
OS_0_3	0	0.49	15.11	24.82	3.97	1261
OS_30_1	30	0.51	15.07	24.88	3.92	1223
OS_30_2	30	0.49	15.11	24.98	3.94	1358
OS_30_3	30	0.49	15.02	24.86	3.94	1220
OS_45_1	45	0.50	15.05	24.89	4.01	1285
OS_45_2	45	0.48	14.94	24.78	3.99	1225
OS_45_3	45	0.47	14.99	24.85	4.00	1174

Table 3. Summary of the experimental results generated by testing the specimens containing open notches (Figs 2i to 2l) under tensile loading.

Code	θ_P [°]	R [mm]	w_n [mm]	w_g [mm]	t [mm]	F_f [N]
BUS_0_1	0	0.04	15.18	24.99	4.02	500
BUS_0_2	0	0.04	15.15	24.92	4.03	519
BUS_0_3	0	0.05	15.21	24.88	4.03	552
BUS_30_1	30	0.05	15.20	24.98	3.93	394
BUS_30_2	30	0.04	15.14	24.89	4.00	395
BUS_30_3	30	0.06	15.17	24.99	3.98	411
BUS_45_1	45	0.05	15.16	25.04	3.96	397
BUS_45_2	45	0.06	15.14	25.01	3.96	406
BUS_45_3	45	0.06	15.16	24.96	3.99	470
BUI_0_1	0	0.95	15.00	24.87	3.96	556
BUI_0_2	0	0.98	14.99	24.92	3.95	620
BUI_0_3	0	0.95	15.01	24.86	4.02	542
BUI_30_1	30	0.96	15.03	24.90	4.00	488
BUI_30_2	30	0.96	15.01	24.91	3.96	491
BUI_30_3	30	0.97	14.98	24.95	3.93	438
BUI_45_1	45	0.94	15.12	25.00	3.96	460
BUI_45_2	45	0.95	15.09	24.96	3.95	450
BUI_45_3	45	0.96	15.12	25.01	3.97	434
BUB_0_1	0	2.96	14.99	24.92	3.94	594
BUB_0_2	0	2.98	15.02	24.85	3.96	442
BUB_0_3	0	2.95	14.95	24.87	3.95	550
BUB_30_1	30	2.95	14.98	24.92	3.89	442
BUB_30_2	30	2.93	14.99	24.94	3.96	454
BUB_30_3	30	2.95	14.97	24.94	3.99	444
BUB_45_1	45	2.99	14.98	25.00	3.96	455
BUB_45_2	45	2.95	14.97	24.92	3.93	435
BUB_45_3	45	2.96	15.02	24.93	4.03	433

Table 4. Summary of the experimental results generated by testing the notched specimens (Figs 2f to 2h) under three-point bending.

Code	θ_P	R	w_n	w_g	t	F_f
	[°]	*[mm]*	*[mm]*	*[mm]*	*[mm]*	*[N]*
BVS_0_1	0	0.32	15.13	24.95	4.03	463
BVS_0_2	0	0.35	15.18	24.95	3.95	419
BVS_0_3	0	0.33	15.15	25.01	4.01	488
BVS_30_1	30	0.32	15.03	24.94	3.94	385
BVS_30_2	30	0.34	15.08	25.02	3.96	401
BVS_30_3	30	0.36	14.95	24.88	3.95	368
BVS_45_1	45	0.38	14.99	24.98	3.96	329
BVS_45_2	45	0.40	15.06	24.96	3.96	345
BVS_45_3	45	0.36	15.06	24.90	3.96	359
BVI_0_1	0	0.98	15.15	24.98	3.97	462
BVI_0_2	0	1.01	15.18	24.99	3.98	454
BVI_0_3	0	1.03	15.13	24.99	3.95	420
BVI_30_1	30	0.96	15.03	24.90	3.99	336
BVI_30_2	30	1.02	15.03	24.91	4.00	394
BVI_30_3	30	1.04	15.14	25.00	3.99	385
BVI_45_1	45	1.01	15.16	24.92	3.97	399
BVI_45_2	45	1.02	15.07	25.00	3.92	387
BVI_45_3	45	1.00	15.13	24.93	3.92	398
BVB_0_1	0	3.03	15.06	25.00	4.02	452
BVB_0_2	0	3.00	15.08	25.06	3.94	451
BVB_0_3	0	3.01	15.15	25.04	3.92	486
BVB_30_1	30	3.02	15.14	25.01	3.91	368
BVB_30_2	30	3.01	15.10	25.06	3.96	392
BVB_30_3	30	3.02	15.01	24.92	3.96	352
BVB_45_1	45	3.01	15.08	25.11	3.96	366
BVB_45_2	45	3.00	15.05	24.88	3.91	372
BVB_45_3	45	3.01	15.13	24.85	3.96	379

Table 5. Summary of the experimental results generated by testing the specimens containing open notches (Figs 2m to 2o) under three-point bending.

Code	θ_P	B	W	a	P_{max}	P_Q	K_C
	[Deg]	*[mm]*	*[mm]*	*[mm]*	*[N]*	*[N]*	*[MPa·m$^{1/2}$]*
CT_45_1	45	29.8	59.89	30.02	1914	1831	2.4
CT_45_2	45	29.9	59.92	30.01	1987	1982	2.6
CT_45_3	45	29.8	60.01	30.01	2164	2119	2.8
CT_45_4	45	25.1	59.96	29.98	1553	1516	2.4
CT_45_5	45	7.3	60.01	29.96	465	436	2.4

Table 6. Summary of the experimental results generated by testing the C(T) specimens (Fig. 2b).

Code	Load Type	θ_P	Opening Angle	Nominal Dimensions				F_f	
				R	w_n	w_g	t	Average	S_D
		[Deg]	*[Deg]*	*[mm]*	*[mm]*	*[mm]*	*[mm]*	*[N]*	*[N]*
UB_0		0						1521	266
UB_30	Tension	30	0	3	15	25	4	1378	86
UB_45		45						1368	144
UI_0		0						1793	42
UI_30	Tension	30	0	1	15	25	4	1402	98
UI_45		45						1326	197
US_0		0						1199	352
US_30	Tension	30	0	0.5	15	25	4	1221	66
US_45		45						1219	120
OB_0		0						1210	225
OB_30	Tension	30	135	3	15	25	4	1284	84
OB_45		45						1412	99
OI_0		0						1492	67
OI_30	Tension	30	135	1	15	25	4	1410	40
OI_45		45						1253	101
OS_0		0						1333	63
OS_30	Tension	30	135	0.5	15	25	4	1267	79
OS_45		45						1228	55
BUB_0		0						529	78
BUB_30	Bending	30	0	3	15	25	4	447	6
BUB_45		45						441	12
BUI_0		0						573	41
BUI_30	Bending	30	0	1	15	25	4	472	30
BUI_45		45						448	13
BUS_0		0						524	26
BUS_30	Bending	30	60	0.5	15	25	4	400	10
BUS_45		45						424	39
BVB_0		0						463	20
BVB_30	Bending	30	135	3	15	25	4	371	20
BVB_45		45						372	7
BVI_0		0						445	22
BVI_30	Bending	30	135	1	15	25	4	371	31
BVI_45		45						395	6
BVS_0		0						457	35
BVS_30	Bending	30	135	0.4	15	25	4	384	17
BVS_45		45						344	15

Table 7. Experimental results generated by testing the notched specimens summarised in terms of average and standard deviation, S_D, of the failure force, F_f.

Figures

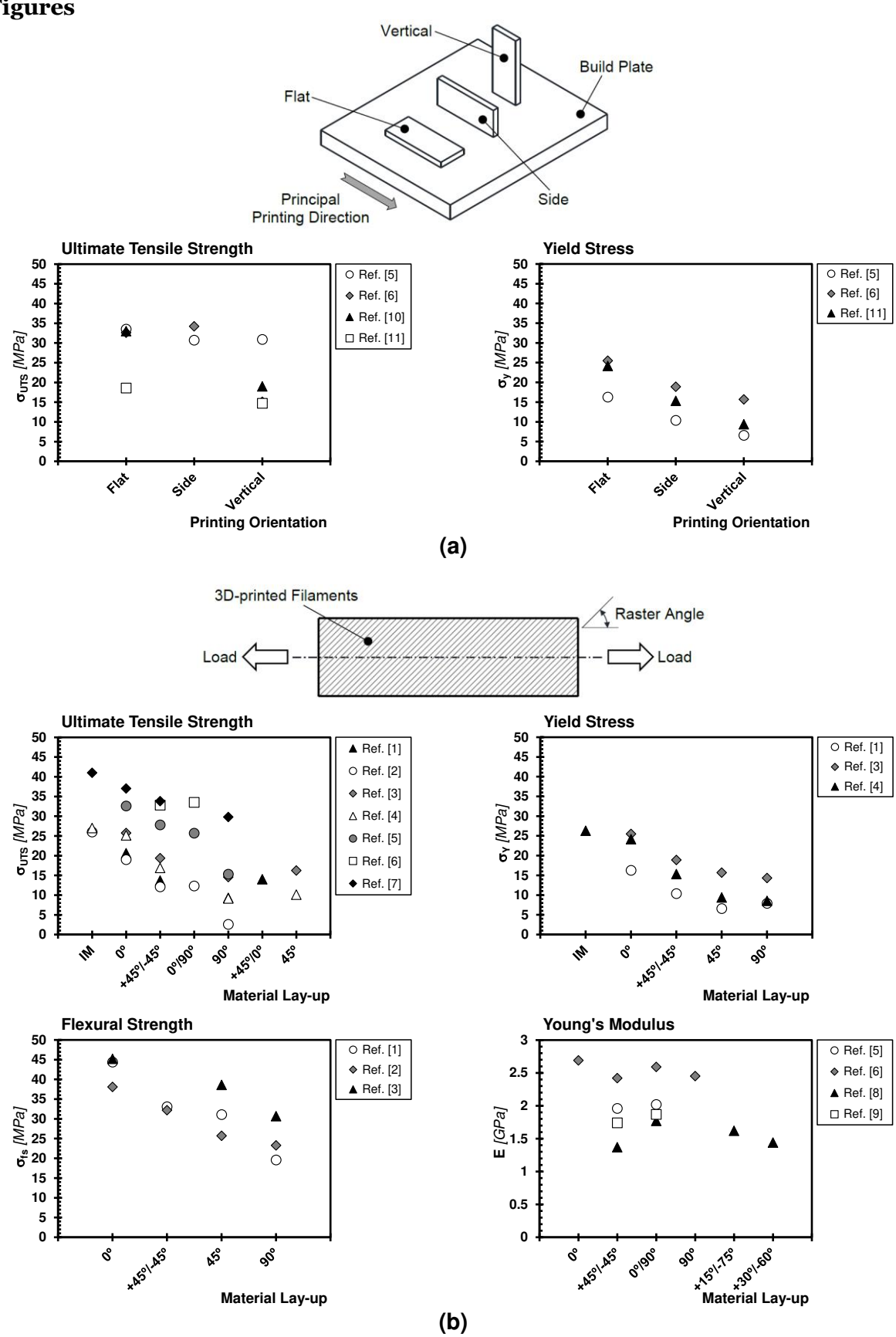

Figure 1. Influence of manufacturing direction (a) and material lay-up (b) on the mechanical behaviour of 3D-printed ABS.

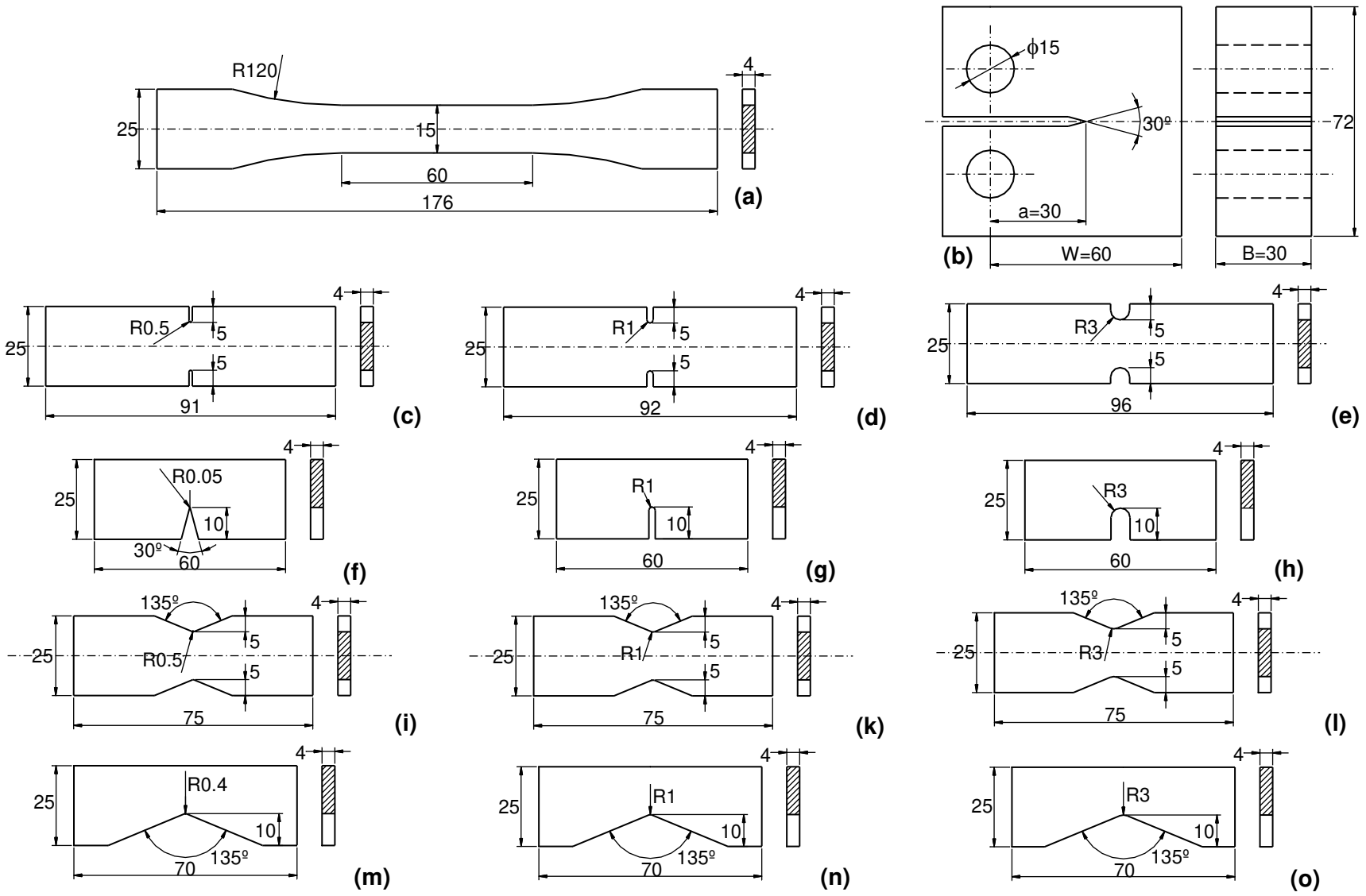

Figure 2. Geometries of the tested specimens (nominal dimensions in millimetres).

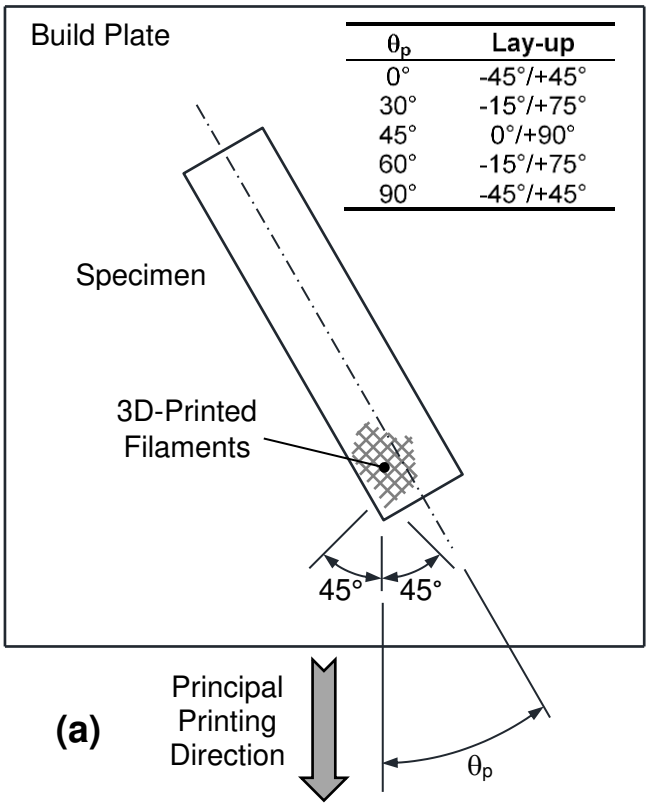

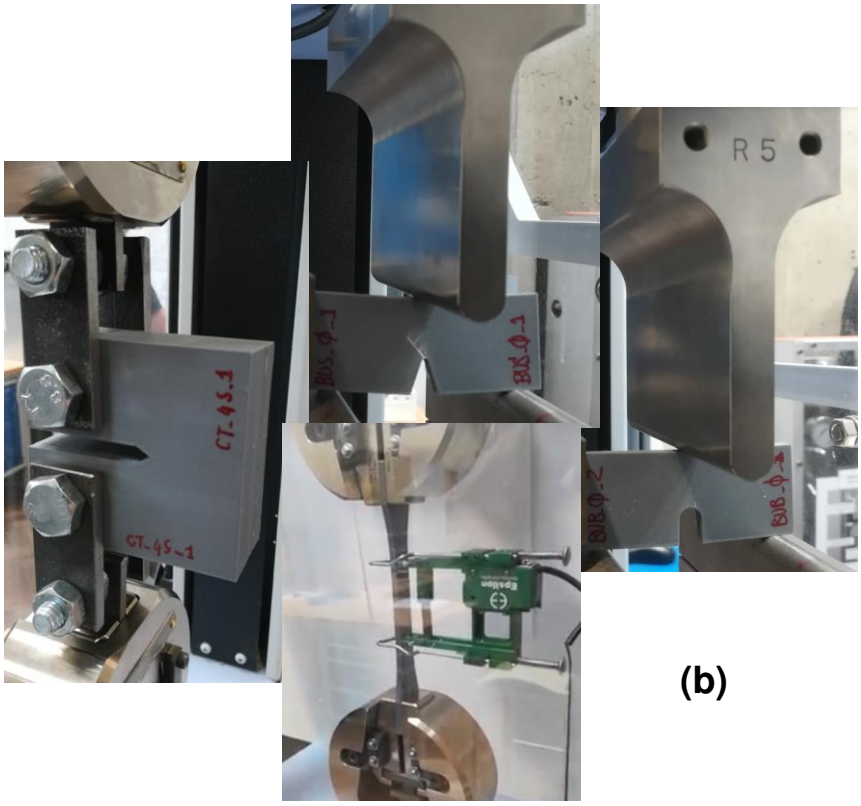

Figure 3. Definition of manufacturing angle θ_p and orientation of the 3D-printed filaments with respect to the specimen axis (a); examples of used testing set-ups (b).

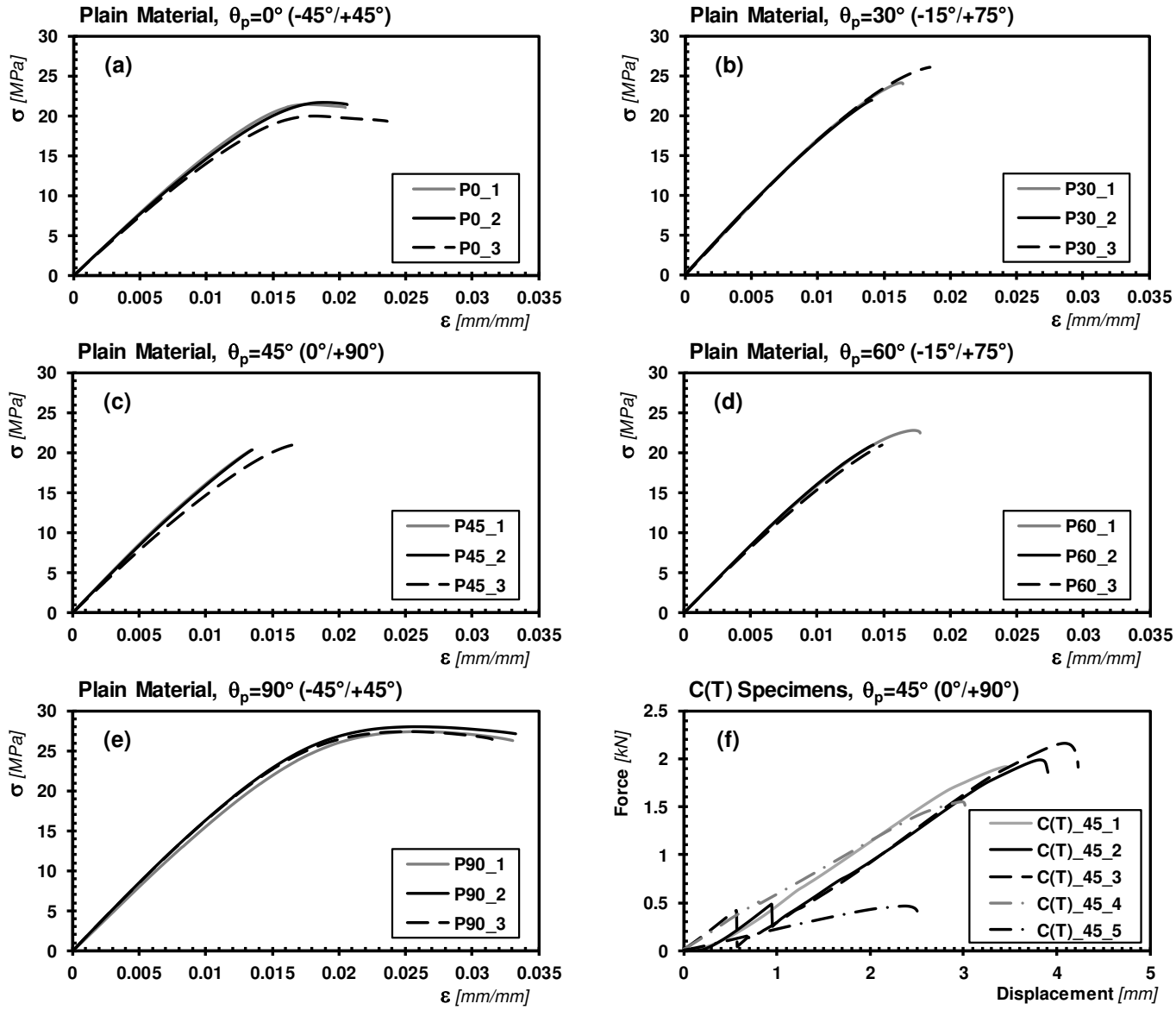

Figure 4. Stress vs. strain curves generated by testing the plain samples under tensile loading (a-e); force vs. displacement curves generated by testing the C(T) specimens (f).

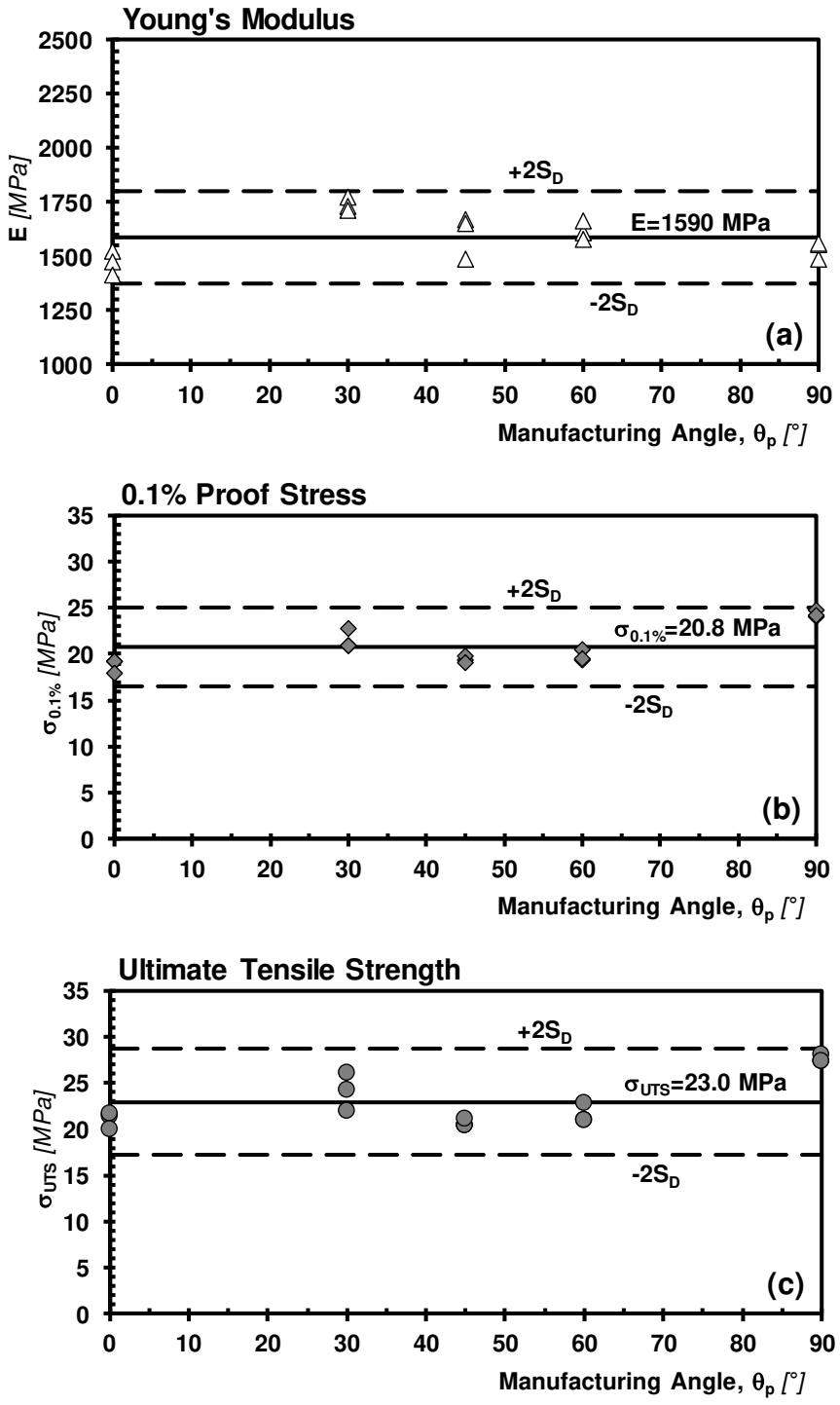

Figure 5. Influence of manufacturing angle θ_p on Young's modulus (a), 0.1% proof stress (b) and ultimate tensile strength (c).

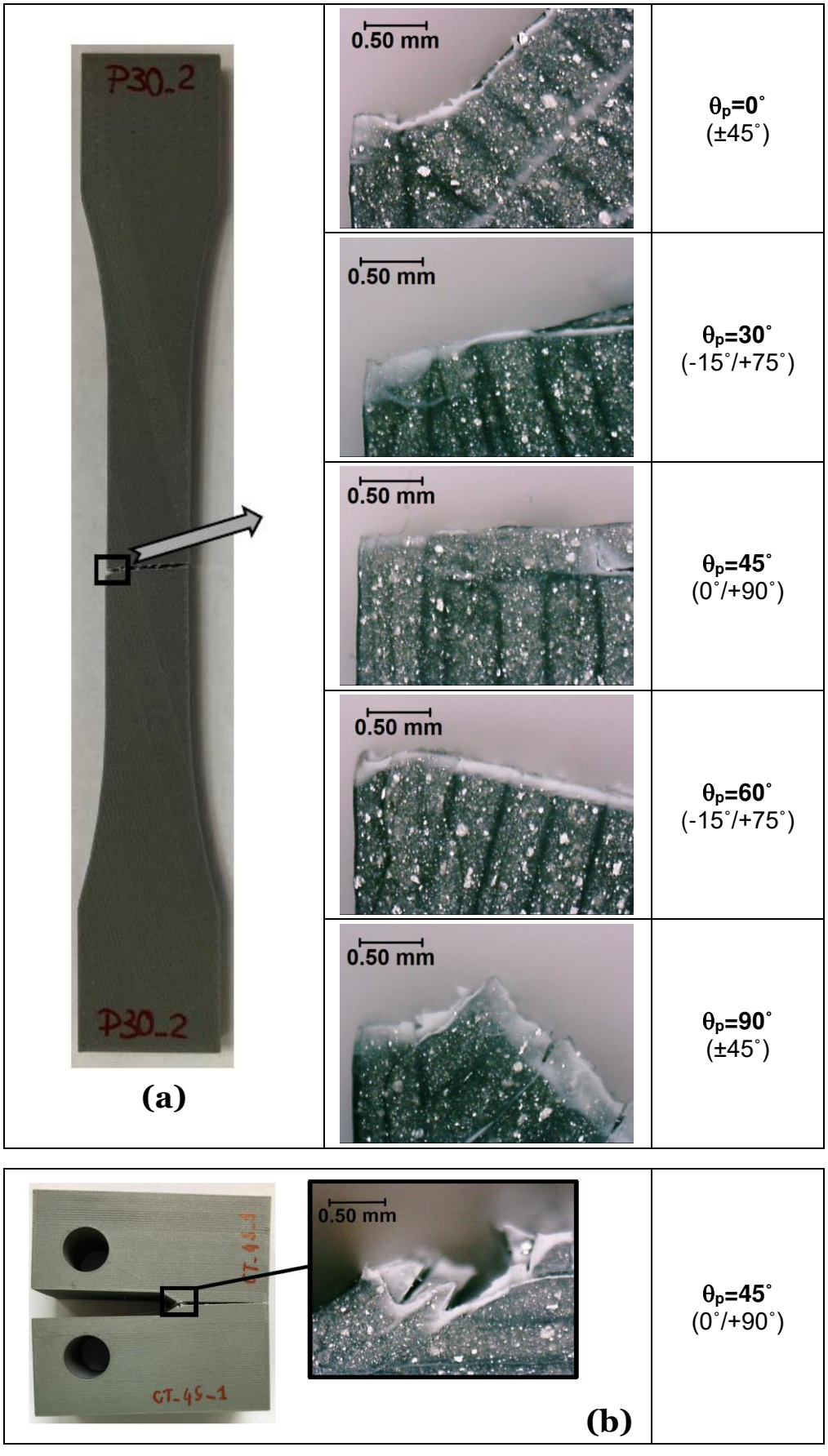

Figure 6. Examples of the cracking behaviour displayed by the plain specimens (a) and by the C(T) specimens (b).

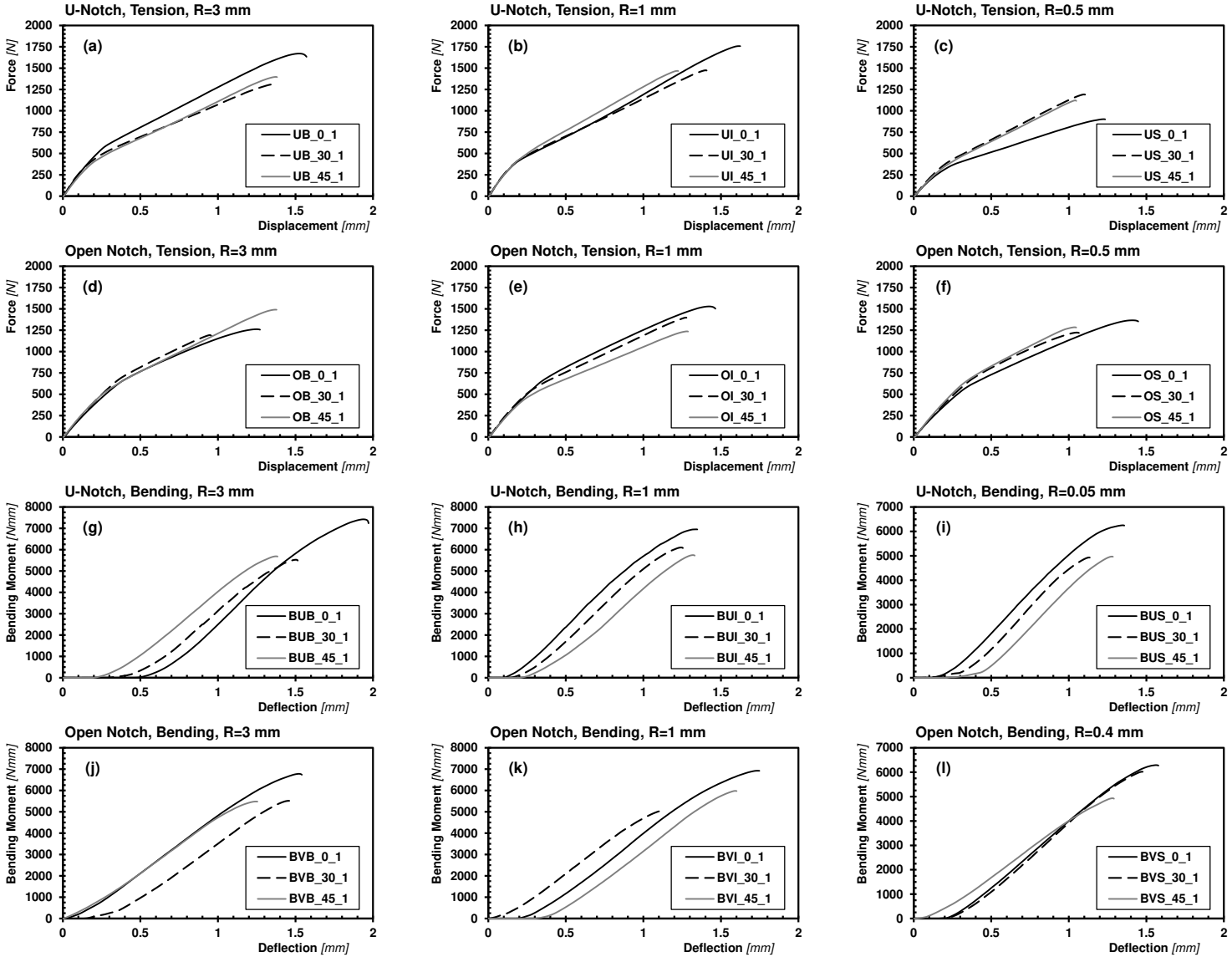

Figure 7. Examples of the mechanical behaviour displayed the notched specimens under tensile (a-f) and bending loading (g-m).

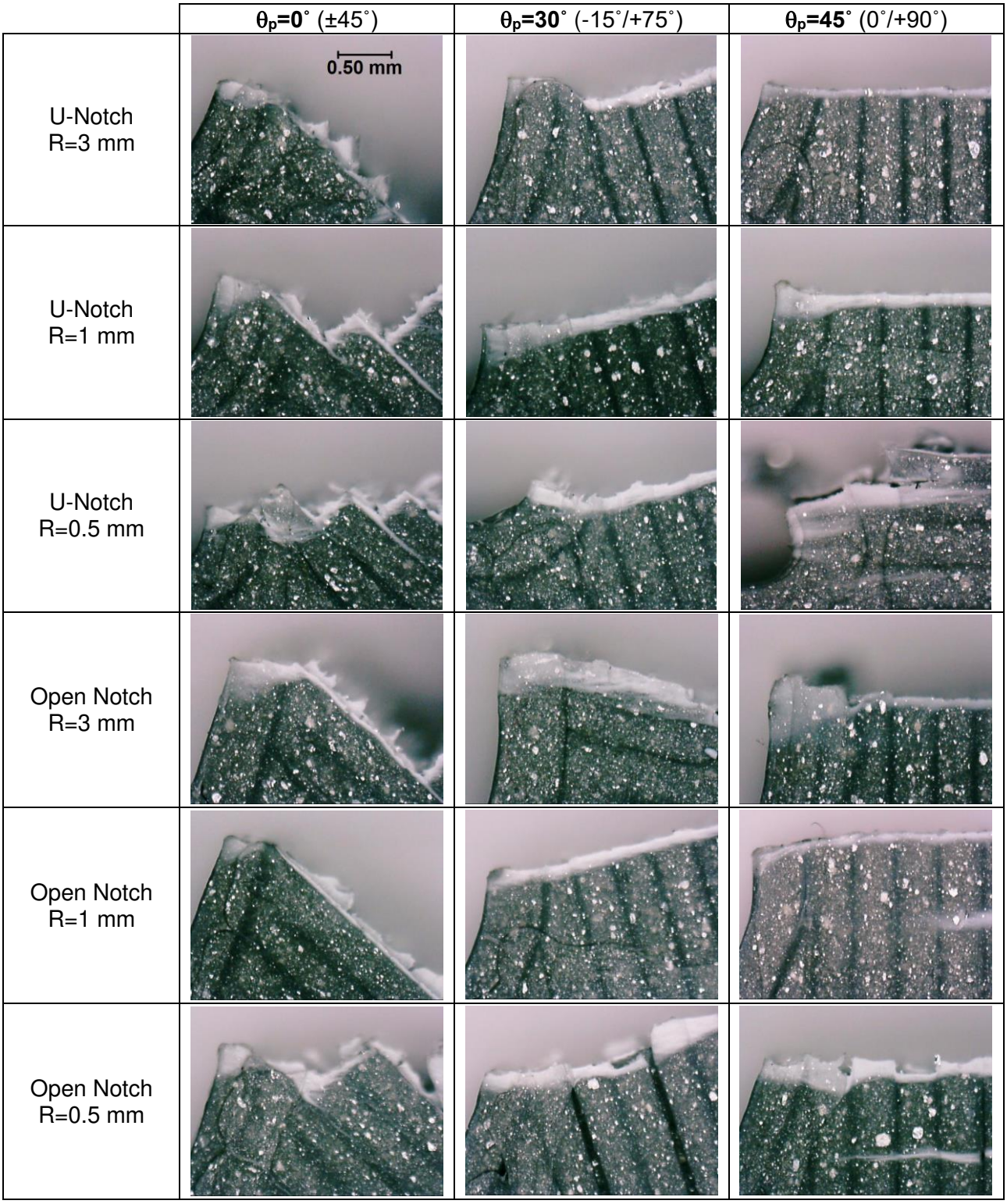

Figure 8. Cracking behaviour displayed by the notched specimens tested under tension (in the pictures the specimen's longitudinal axis is vertical and the notch tip on the left-hand side).

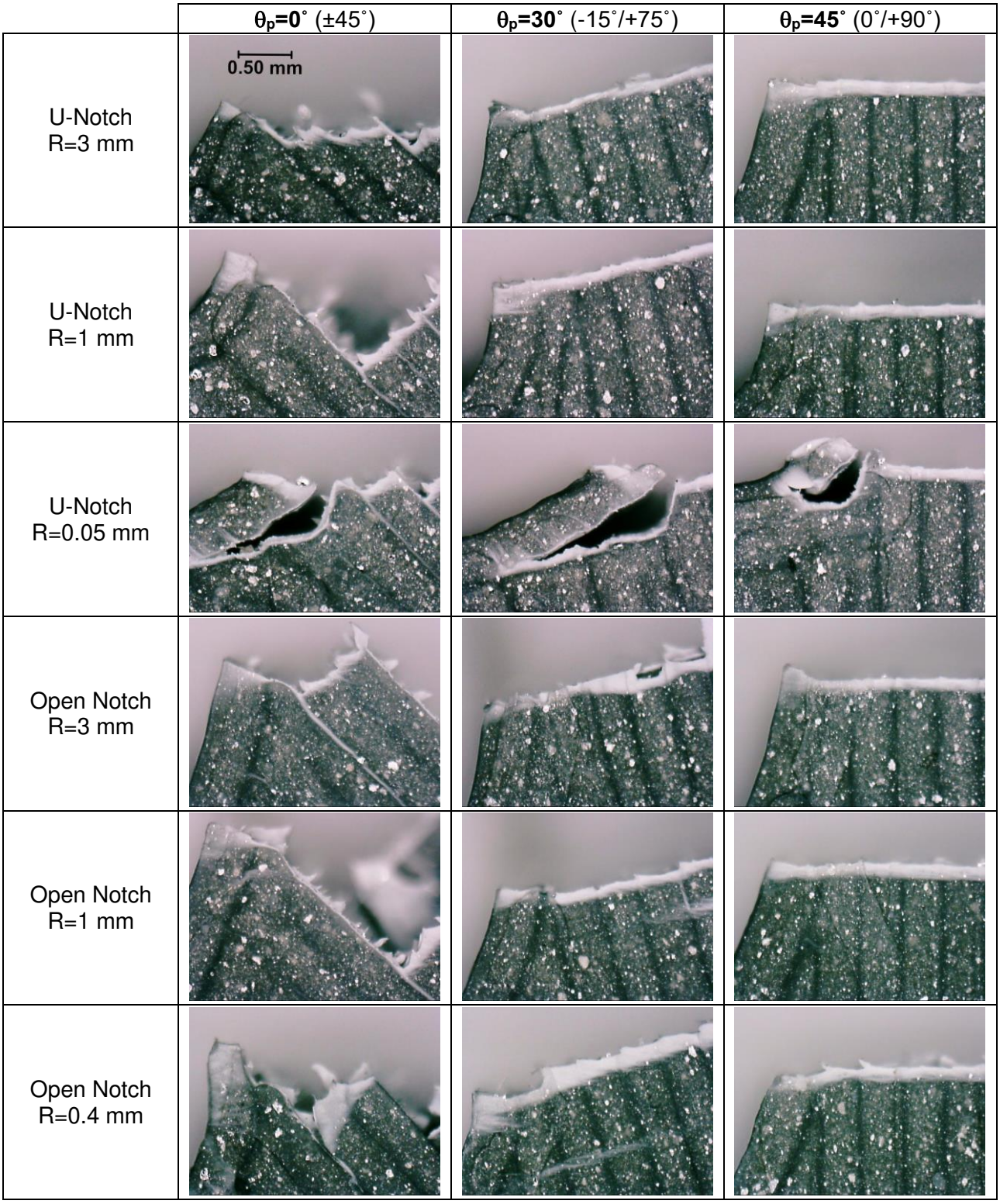

Figure 9. Cracking behaviour displayed by the notched specimens tested under three-point bending (in the pictures the specimen's longitudinal axis is vertical and the notch tip on the left-hand side).

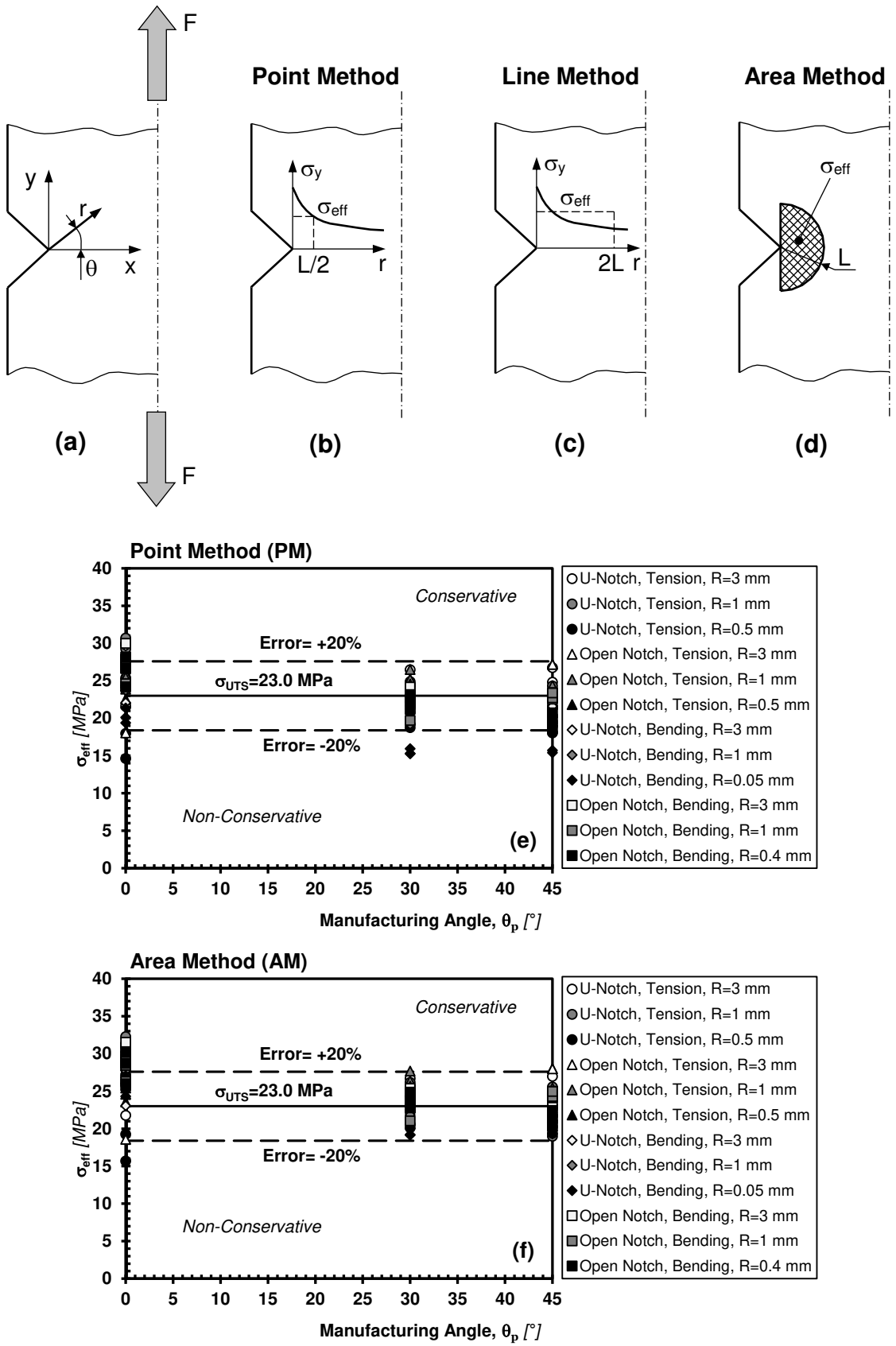

Figure 10. Notched components loaded in tension (a); effective stress determined according to the Point (b), Line (c), and Area Method (d); accuracy of the TCD used in the form of the Point (a) and Area Method (b) in estimating the notch static strength of the 3D-printed ABS being tested.